Synthesis and Atomic Scale Investigation of Borophene on Au(111)

A thesis submitted towards partial fulfilment of
BS-MS Dual Degree Programme

By

Navathej P Genesh

(BS-MS student, Registration No.: 20121004)

Under the guidance of

Dr. Aparna Deshpande

Department of Physics
Indian Institute of Science Education and Research (IISER) Pune, India

Certificate

This is to certify that this dissertation entitled **"Synthesis and atomic scale investigation of borophene on Au(111)"** towards the partial fulfillment of the BS-MS dual degree programme at the Indian Institute of Science Education and Research Pune, represents original research carried out by **Navathej P Genesh** at IISER Pune under the supervision of **"Dr. Aparna Deshpande**, Assistant Professor, Department of Physics, IISER Pune" during the academic year of 2016-2017.

Date: 23/03/2017

Place: Pune

Dr. Aparna Deshpande

Assistant Professor

Department of Physics

IISER Pune

Declaration by the candidate

I hereby declare that the matter embodied in the report entitled "**Synthesis and atomic scale investigation of borophene on Au(111)**" are the results of investigation carried out by me at the Department of Physics, IISER Pune, Under the supervision of Dr. Aparna Deshpande and the same has not been submitted elsewhere for any other degree.

Navathej P Genesh

Date: 23/03/2017

Place: Pune

<u>Acknowledgements</u>

TABLE OF CONTENTS

LIST OF FIGURES

LIST OF TABLES

LIST OF ABBREVIATIONS

AFM – Atomic Force Microscope

EDAX – Energy Dispersive X-Ray Spectroscopy

LT – Low temperature

STM – Scanning Tunnelling Microscope

UHV – Ultra High Vacuum

ABSTRACT

Boron has the ability to form low dimensional allotropes like carbon. So the existence of a two dimensional material consisting of only boron atoms (borophene) was predicted. Recently borophene was synthesized on Ag(111) in two parallel experiments. This project is the study of boron nanostructure on Au(111) substrate. Atomic scale investigation of boron nanostructures on Au(111) was carried out using ultra high vacuum-low temperature STM at 77 K. Boron nanostructures showed different morphologies with change in boron flux, exposure time and substrate temperature during deposition. Boron deposition became more planar with reduction in exposure time and increase in substrate temperature.

INTRODUCTION

1.1 Introduction

During the course of history scientific research and technological advancements have played a pivotal role in shaping our lives. Discovery of electromagnetic induction by Michel Faraday led to the production of electricity. His discovery remains one of the most influential scientific breakthroughs even after two centuries. With time the realms of science got broadened, bringing along with it diverse problems. Fossil fuels and electricity are the major source of energy these days, but most of this energy comes from non renewable energy sources. With ever increasing energy need the quest for alternate energy sources has become one of the serious problems that science has to address. Recently environmental issues have raised the need for sustainable, green, and renewable energy sources.[1] In order to tackle this ever growing energy need the study of materials and their properties have a lot to offer. Efficient energy production and transmission requires more understanding of the basic properties of materials. The field of condensed matter physics aims to understand the material world around us.

1.2 Two Dimensional Materials

The discovery of two dimensional (2D) materials was one of the remarkable scientific achievements in recent times. Graphene, a material with honey comb lattice of carbon atoms was the first 2D material to get isolated. This was done by A K Geim and K S Novoselov for which they received Nobel prize for physics in 2010.[2] Graphene has a high electric mobility and thus the charge carriers in graphene behave like relativistic particles which are termed as Dirac fermions. In condensed matter most of the systems are modelled by Schrodinger equation where as in the case of graphene Dirac equation is used to model the system due to the relativistic speed of charge carriers in them.[2] Due to graphene's high electrical conductivity and large surface to volume ratio graphene powder can be used in batteries which will improve its efficiency.[2] Many other two dimensional materials were also discovered after graphene namely, MoS_2, phosphorene, hexagonal boron nitride, etc. Motivated by the similarities between carbon and boron, borophene a new two dimensional material consisting of boron atoms was synthesized by Mannix, et.al.[18]

1.3 Boron

Boron is an element of group 13 with an atomic number 5. It has an electronic distribution $1s^2$, $2s^2$, $2p^1$ with a melting point of 2300^0C.[3] The chemistry of boron has been investigated widely. [4][5][6][7] There are 16 allotropes of boron reported so far. α-Rhombohedral, β-Rhombohedral, α-Tetragonal, β-Tetragonal and γ-Orthorhombic are some crystalline allotropes. Powder boron and glassy boron are amorphous allotropes of boron. These allotropes have icosahedral B_{12} units, fused icosahedra and small interstitial clusters. [7]

Boron forms various low dimensional allotropes like carbon (fullerenes, nanotubes, 2D sheets) due to the same short covalent radius and ability to form sp^2 hybridized orbitals as carbon. There are many examples to site in this regard. First one is the all boron fullerene (B_{40}) which was synthesized in 2014. All boron fullerene had 40 vertices, 92 edges, 48 triangular faces, 2 hexagonal faces and 4 heptagonal faces.[8] Similar to carbon, boron also forms boron nanotubes. [17] The next question that arises is whether a 2D material similar graphene can be synthesized out of boron. The structure and stability of boron clusters were studied in detail. It was predicted that pure boron clusters continue to be planar or quasi planar up to 24 atoms.[10] Neutral B_{36}, the smallest boron cluster to show six-fold symmetry was reported by Zachary A. Piazza et.al. It is a highly stable quasi planar boron cluster with hexagonal hole. [9] During this experiment boron cluster anions were produced from boron target made of Boron powder. Laser vaporisation technique was used for this purpose. Formed clusters were extracted and analysed by mass spectrometer. Clusters of interest were mass selected and photo electron spectroscopy was carried out. Theoretical modelling of the obtained photo electron spectrum was done to predict the structure of the cluster. Repeated B_{36} units can give rise to 2D boron sheets (borophene) as shown in figure 1.1. However the formation of boron sheets from B_{36} clusters is not experimentally verified yet.
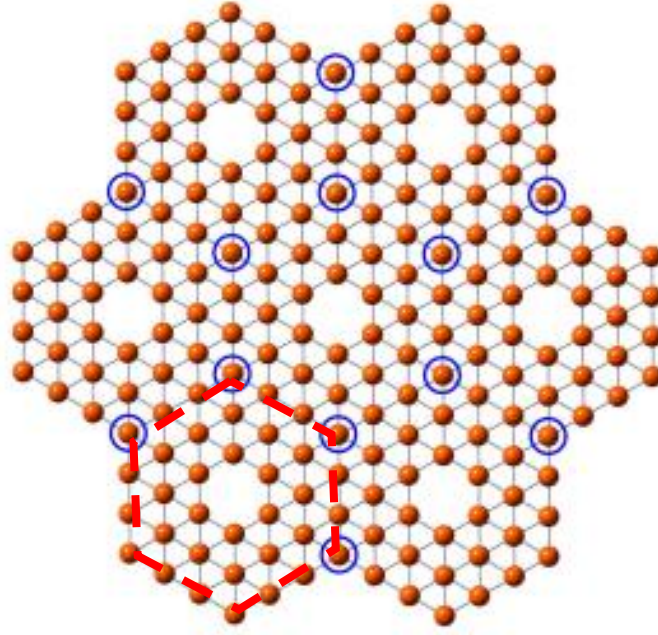
Figure 1.1 A predicted boron sheet structure made up of B_{36} units. Red line represents one B_{36} unit. Circled atoms at the apex of B_{36} units are shared by three neighbouring units.[9]

1.4 Borophene

Experimental studies on nano-structured boron allotropes are very less whereas there a lot of theoretical studies based on 2D boron sheets. Although these studies predict different structures for 2D boron sheets, borophene is used as a general name for them. Hui Tang et.al. have shown that two and three centred bond formation in pure boron compounds which can enhance the stability of boron sheets.[11] It was also shown that out-of-plane distortions can also enhance the stability boron sheets.[12][13] Borophene is predicted to be in metallic or semi-metallic forms.[12][14] There are a lot of theoretically predicted structures of borophene named as α sheets, β sheets, χ and δ sheets classified on the basis of connectivity of boron atoms.[22] Figure 1.2 shows the different types of 2D boron sheets. The coordination number of boron atoms varies from one type of sheet to another. Some 2D boron structures are predicted to host Dirac fermions like graphene.[12]
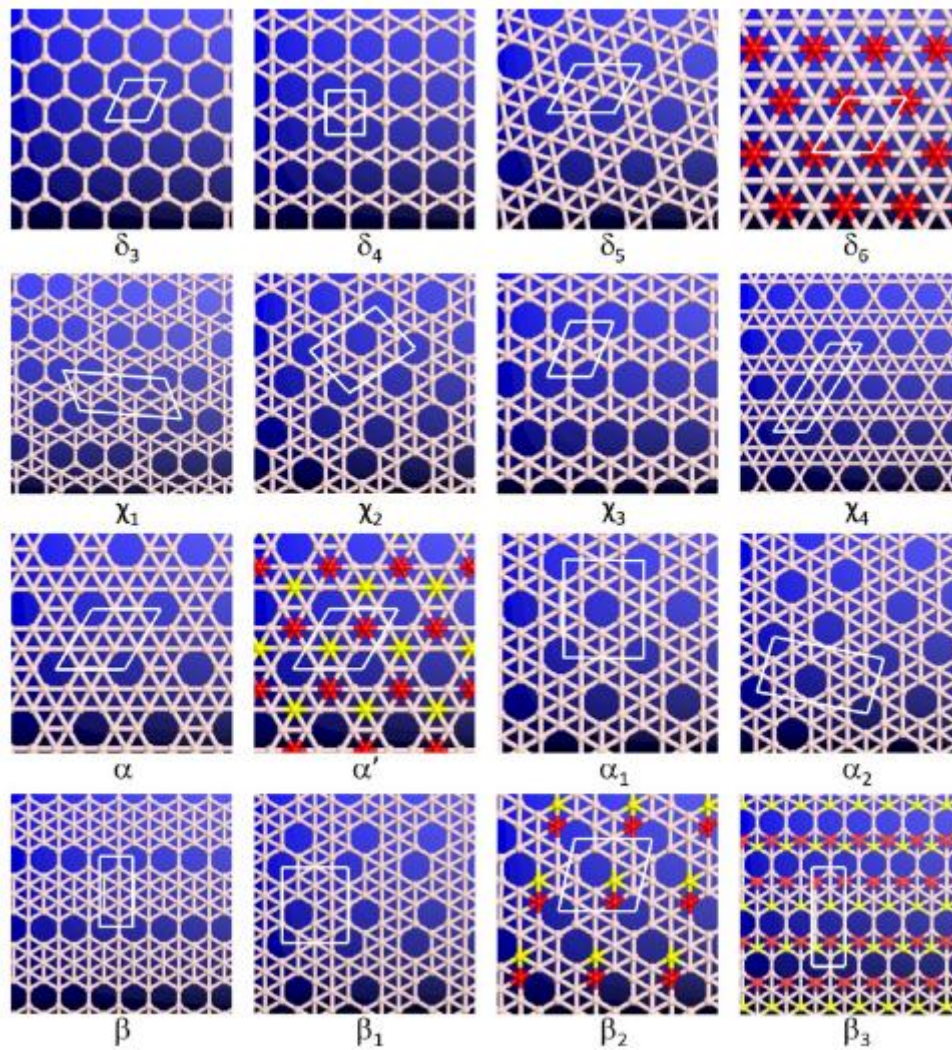
Figure 1.2 A top view of the δ, α, β and χ boron monolayer sheets. These are the low energy structures predicted by DFT calculations. Yellow and blue colour represents boron atoms sitting inside and outside the plane of the sheet. [22]

Borophene has been recently grown on single crystal Ag(111) substrate. This was carried out in two parallel experiments.[18][19] Although there are many stable structures predicted for the boron sheets, they observed only β_{12}, χ_3 and striped phases of borophene. β_{12} and χ_3 phases were having planar structure with periodic holes. Striped phase has anisotropic corrugations and buckled structure. All these phases showed metallic character. [18][19] Low deposition rate preferred striped phase where as high deposition rate preferred homogenous phase which can either be β_{12} or χ_3 phase.[18][19] High substrate temperature preferred χ_3 phase over β_{12}. High temperature also favoured striped phase over homogenous phase, which suggests that

homogenous phase is a metastable state. [18][19] Recently Dirac fermions are predicted on β_{12} boron sheets. [21] A J Mannix et.al. were able to show that borophene can sustain periodic undulations on reconstructed Ag(111). This was done using theoretical calculations and STM images with atomic resolution of borophene.[20]
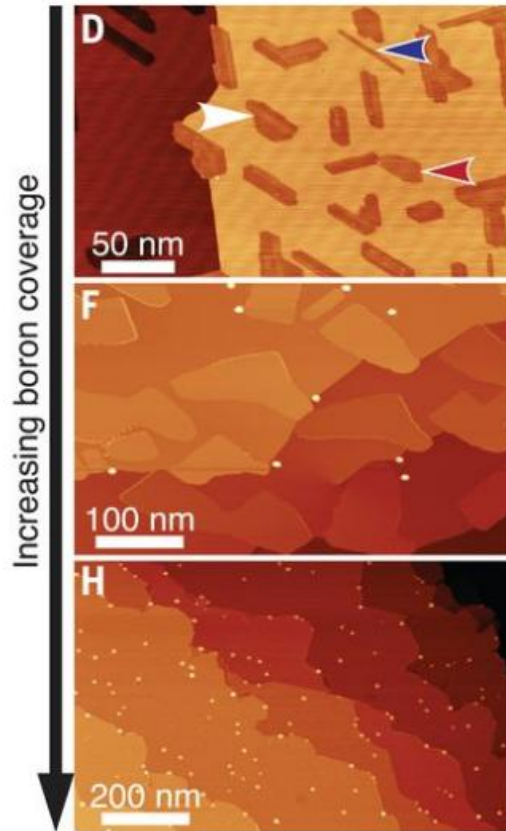

Figure 1.3 STM images of Borophene grown on Ag(111) at low, medium and high coverage. Low coverage resulted in the formation of striped phase and high coverage resulted in homogenous phase[18]

Borophene is expected to form weak binding and show anisotropic growth when adsorbed on to a noble-metal surface (Ag(111), Au(111) and Cu(111)). [15][16] These calculations were performed by considering chemical potential of the boron sheet over these substrates.[15] Since growth of borophene on Ag(111) has already been investigated, it became more interesting to study the borophene growth on Au(111).

The aim of this project is to synthesize borophene on Au(111) in UHV conditions and to characterize the boron nanostructures formed on Au(111) using LT STM. Since STM can probe the topography and the electronic structures at atomic scale, it can investigate the electronic structures and morphology of the boron nanostructures that are getting formed

15

during the experiments. Different parameters like boron deposition flux, exposure time of the Au(111) substrate to boron flux, and substrate temperature during deposition were controlled to understand the differences in morphology and electronic properties of the boron nanostructures.

-

METHODS

2.1 Scanning Tunnelling Microscope (STM)

In classical mechanics a particle with energy lesser than the potential barrier does not cross the barrier where as in quantum mechanics there is finite probability that it will cross the barrier. This is the basis for quantum mechanical tunnelling.

In quantum mechanics an electron with total energy E in a potential U(z) is described by a wave function $\Psi(z)$, which satisfies the Schrödinger equation. For the special case of E<U, wave function is given by

$$\Psi(z) = \Psi(0)e^{-kz}$$

Where

$$K == \frac{\sqrt{2m(U-E)}}{\hbar}$$

Probability of finding the electron after the potential barrier is

$$|\Psi(z)|^2 = |\Psi(0)|^2 e^{-2kz}$$

By applying a voltage V to the tip of the STM, a net tunnelling current occurs. This is possible due to the flow of electrons from filled states of tip to unfilled states of sample or filled states of sample to unfilled states of tip. The following diagram describes the tunnelling phenomenon in a metal vacuum metal junction. E_n and Ψ_n are the energy and wave function.
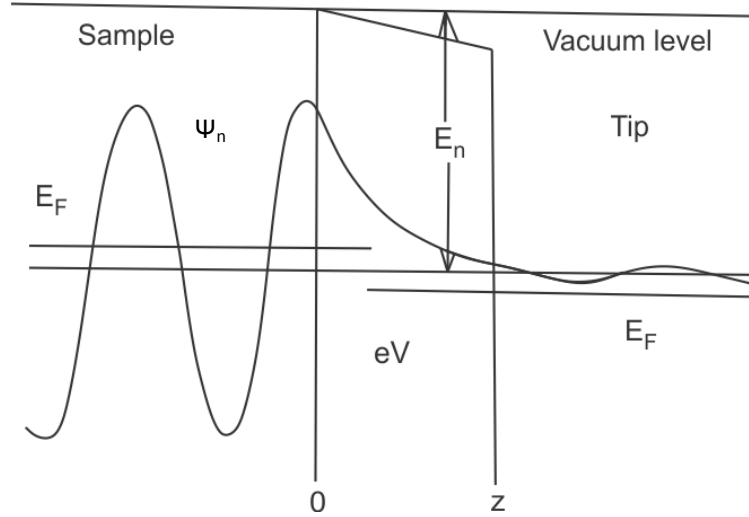
Figure 2.1 Metal vacuum metal junction tunnelling. Tip and sample are considered to be metallic with free electrons in their bulk. A bias V is applied to the sample which makes tunnelling from sample to tip possible. Ψ_n and E_n are the wave function and energy of the sample states. (Adapted from (23))

Here the tunnelling current can be written as

$$I(z)=I(0)e^{-2kz}$$

There are more sophisticated ways to look at this problem. Barden's approach is the following. The direct interaction of electron with tip and interactions amongst tunnelling electrons a-re neglected. Tunnelling current can be written as

$$I = \frac{4\pi e}{\hbar} \int_0^{eV} \rho_s(Ef - eV + \varepsilon) \, \rho_t(Ef + \varepsilon) \, |M|^2 d\varepsilon$$

Where ρ_s and ρ_t are LDOS(local density of states) of sample and tip respectively. E_f is the Fermi energy and V is the bias applied and M is the tunnelling matrix whose elements are

$$M_{\mu v} = \frac{\hbar^2}{2m} \int [\Psi_\mu \frac{\partial \chi_v^*}{\partial z} - \chi_v^* \frac{\partial \Psi_\mu}{\partial x}] \, dxdy$$
$$z=z_0$$

Where Ψ and χ are wave functions of sample and tip respectively.

Assuming the |M| is not changing with respect to energy, then the expression for I becomes

$$I \propto \int_0^{eV} \rho_s(Ef - eV + \varepsilon)\, \rho_t(Ef + \varepsilon)\, d\varepsilon$$

When a sample is scanned with STM a bias is applied between sample and tip. This produces a tunnelling current which will be detected by atomically sharp tip which gets amplified by a preamplifier. The electronics that enables the STM to function is given in the figure. STM can scan in two modes; constant current mode and constant height mode. In constant height mode the tip remains at constant height and the topography variations will be detected by measuring change in the tunnelling current. In constant current mode the feedback loop associated with STM will enable tip scan along a constant current path. Topographic variations will be measured in terms of the movement of piezo along vertical (z) direction. In both the modes tip will do raster scans in x-y plane. Constant current mode is used in most of the cases, where as constant height mode will be used when topographic variations in the sample are very less.

STM can also be used to study the local electronic properties of a material. This technique is called scanning tunnelling spectroscopy (STS). The theory behind STS follows from the expression for tunnelling current. The following expression can be derived from Barden's approach.

$$\left[\frac{dI}{dU}\right]_{U=V} \approx \rho_s(\,E_f + eV\,)\,\rho_t(\,E_f\,)$$

Where ρ_s and ρ_t are the local density of states (LDOS) of both sample and tip respectively. In scanning tunnelling spectroscopy tunnelling current is measured by varying the tip voltage. These values are used to determine $\frac{dI}{dV}$ values corresponding to each voltage. This spectrum gives an idea about the local density of states of the sample for different V values. [23]
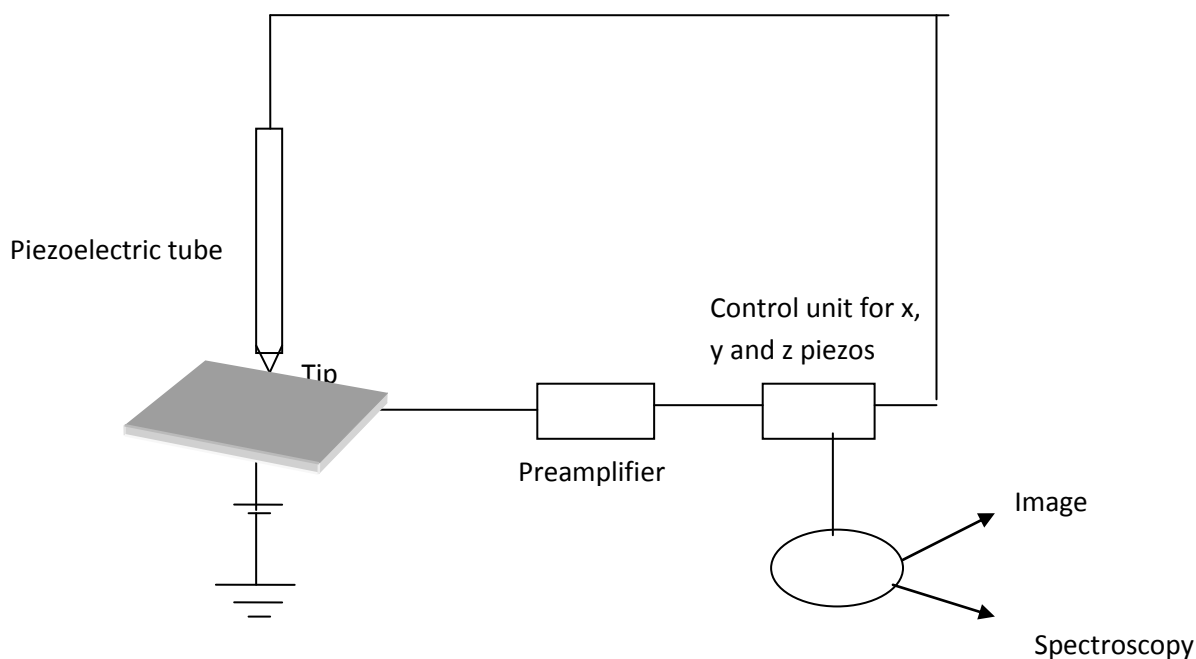
Figure 2.2 STM setup.

2.2 UHV - LT Scanning Tunnelling Microscope: what is UHV and what is LT?

The UHV system that houses the STM has three parts. They are preparation chamber, LT chamber and load lock. LT chamber is kept at low temperature using cryostats which consists of outer liquid nitrogen cylinder and inner liquid helium cylinder. Cryostat helps to maintain the low temperature inside the LT chamber. Both LT chamber and preparation chamber are at ultra high vacuum (UHV) conditions. Ultra high vacuum refers to the pressure lesser than 10^{-7} mbar. This is achieved using an assembly of the rotary pump, turbo molecular pump, ion pump and titanium sublimation pump for both – the preparation chamber and the LT chamber. Molecular evaporator, sputtering unit, heating unit and in situ crystal cleaver are present inside preparation chamber. In preparation chamber heating can be carried out in two ways; direct heating of the sample or indirect heating by tungsten filament. Sample is inserted or taken out of the system via Load Lock where pressure is brought down with the help of Rotary Pump and Turbo Molecular Pump. Pressure in the preparation chamber and LT chamber are measured using ion gauges where as in the load lock pressure is measured using a pirani gauge. In this project ultra high vacuum condition is required for sample preparation. UHV condition prevents the contamination of the sample and facilitates uniform evaporation of molecules and atoms during physical vapour deposition. Scanning Tunnelling Microscope is inside the LT chamber.
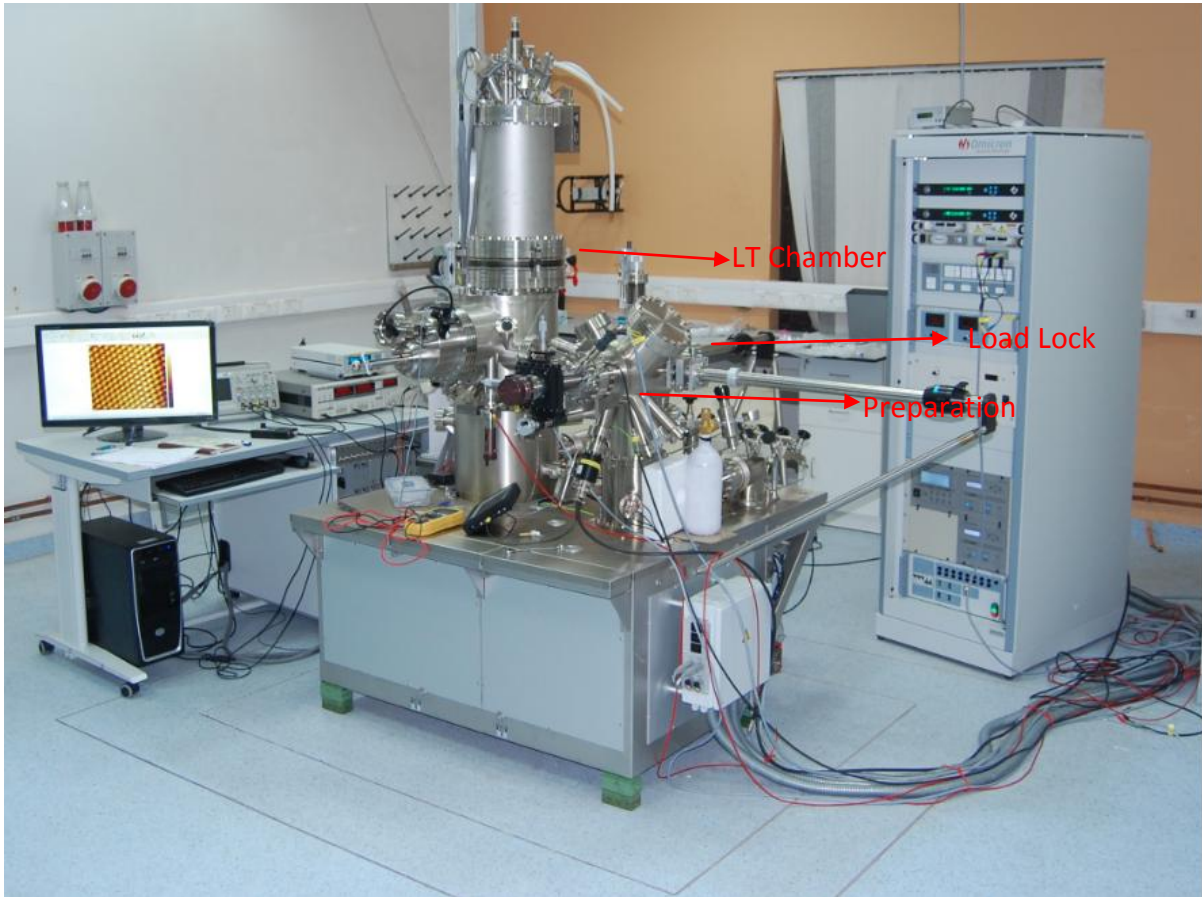
Figure 2.3 UHV-LT STM with three parts: LT chamber, preparation chamber and load lock.

2.3 Rotary Pump

Rotary pump produces pressure down to 10^{-2} to 10^{-3} mbar. Figure 2.4 shows the cross section of a rotary vane pump. Rotor sits in a stator bore which has the same curvature. There are two rotor blades attached to the rotor in diametrically opposite directions. Figure 2.5 shows stages in one rotation of the rotor. It includes induction, isolation, compression and exhaust phases. The rotation of the rotor blade compresses the gas inside the bore which results in the opening of exhaust valve and the removal of gas from the chamber. In this way rotary pump reduces the pressure inside the chamber.
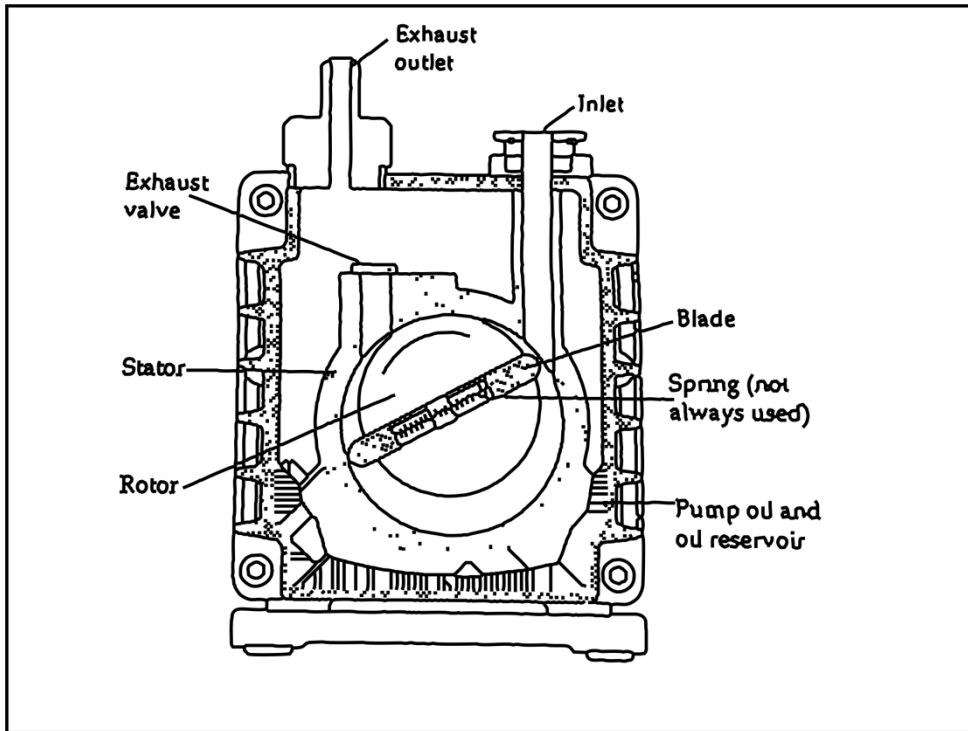
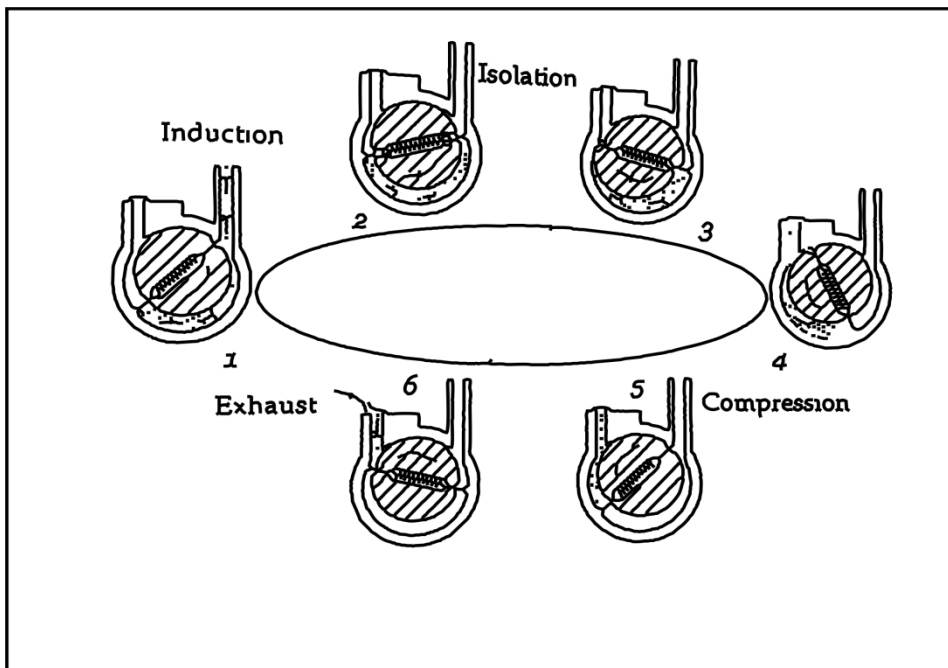**Figure 2.4** A cross sectional view of rotary pump (Adapted from (24))

Figure 2.5 Working of rotary pump (Adapted from (24))

2.4 Turbo Molecular Pump

Turbo molecular pump has got moving blades which are separated by stationary blades. The rotary blades rotate at a very high speed (30,000 revolutions per minute) which helps it to intake and compress gas from high pressure chamber and deliver it to a rotary pump. The minimum pressure it can achieve is of the order of 10^{-9} mbar. The principle behind the turbo molecular pump is the interaction effect between a molecule and moving surface. Figure 2.6 describes in detail how the turbo pump works. The speed of the rotor blade tip is comparable with the average speed of molecules at room temperature. Since lighter molecules travel at a high speed, it is more difficult to remove lighter atoms using turbo molecular pump.
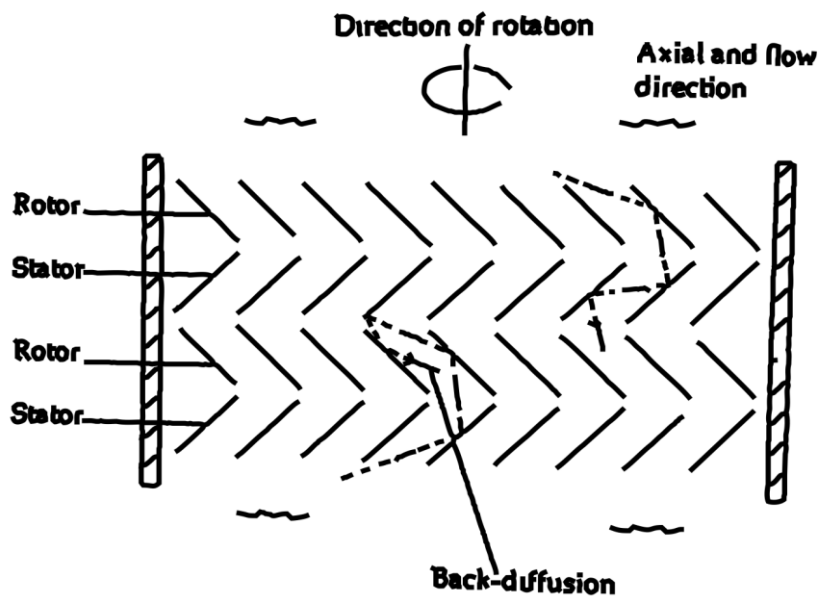
Figure 2.6 Working of Turbo Molecular Pump (Adapted from (24))

2.5 Ion Pump

Ion pump is used to create vacuum of the order of 10^{-8} to 10^{-10} mbar. The pump has a cathode and a chemically active anode (Titanium cathode). An electric potential of the order of 3-7 kV is applied across the electrodes which results in an electric discharge between the electrodes. This creates a swirling cloud of electrons near anode region which ionizes incoming gas molecules and atoms. These ions will hit the chemically active cathode and either become buried or sputter cathode material on to the pump wall. Sputtered cathode acts as a getter which can evacuate the gas by chemisorption or physisorption. Some gas ions can rebound and gain one electron from cathode surface and thus get neutralized. A diagram of ion pump is given in figure 2.7.
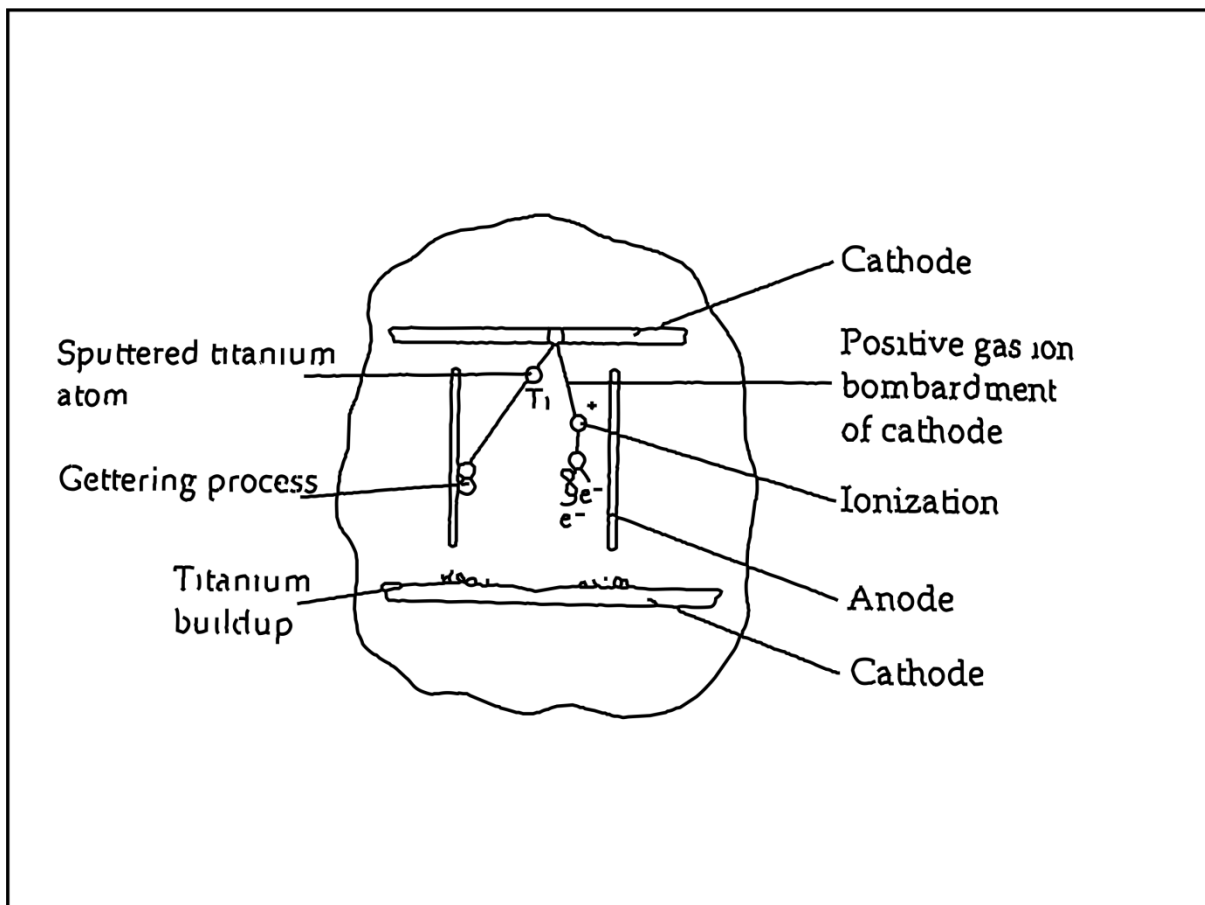

Figure 2.7 Schematic of an ion pump (Adapted from (24))

2.6 Titanium Sublimation Pump (TSP)

Titanium sublimation pump consists of a titanium filament which gets sublimated when a high current is passed through it. When current of almost 40 A is passed through the filament, titanium sublimates and the surrounding chamber walls will get coated with thin layer of clean titanium. Clean titanium is reactive and it reacts with colliding remaining gas in the chamber. Reaction produces solid products, which are stable and thus lower the pressure inside the chamber. The rate of reaction of sublimated titanium depends on surrounding pressure, temperature, period between successive sublimations, composition of the remaining gas, etc.

2.7 Ion Gauge

It works on the basis of ionization of gas molecules by a constant current of electrons. Electrons are emitted at controlled rate from a heater filament which serves as a cathode. These electrons will get accelerated towards a positive wire grid which serves as an anode. The electrons passing through the grid ionizes gas molecules and positive ions are detected by the ion collector that is located along the axis of the cylindrical grid. The strength of the electric current produced is measured by an electrometer which is calibrated in the units of pressure. A diagram of ion gauge is given in figure 2.8. Pressure inside preparation chamber and LT chamber are measured using ion gauge.
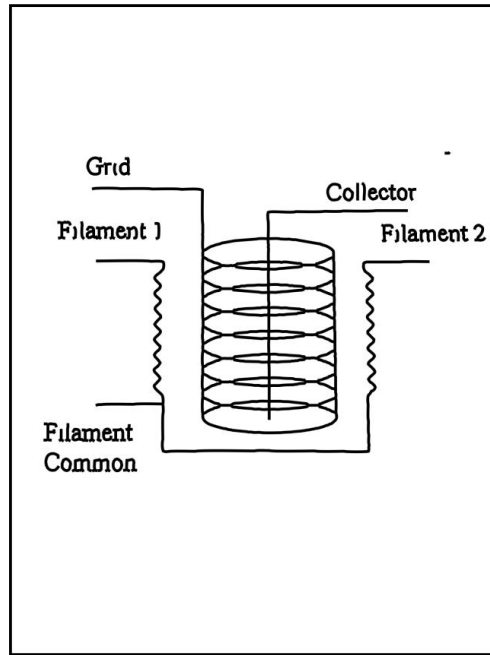
Figure 2.8 Schematic of an ion gauge

2.8 Pirani Gauge

Pirani gauge is an example for thermal conductivity gauge. A diagram of pirani gauge is given in figure 2.9. The conducting filament gets heated when current flows through it. Since the filament is surrounded by gas molecules, it loses heat when gas molecules collide with the filament. Thus the temperature of the filament is an indicator of the pressure inside the chamber. Current that balances the bridge is also measured. This gives the value of the pressure inside the chamber. Pressure inside the load lock is measured using pirani gauge.
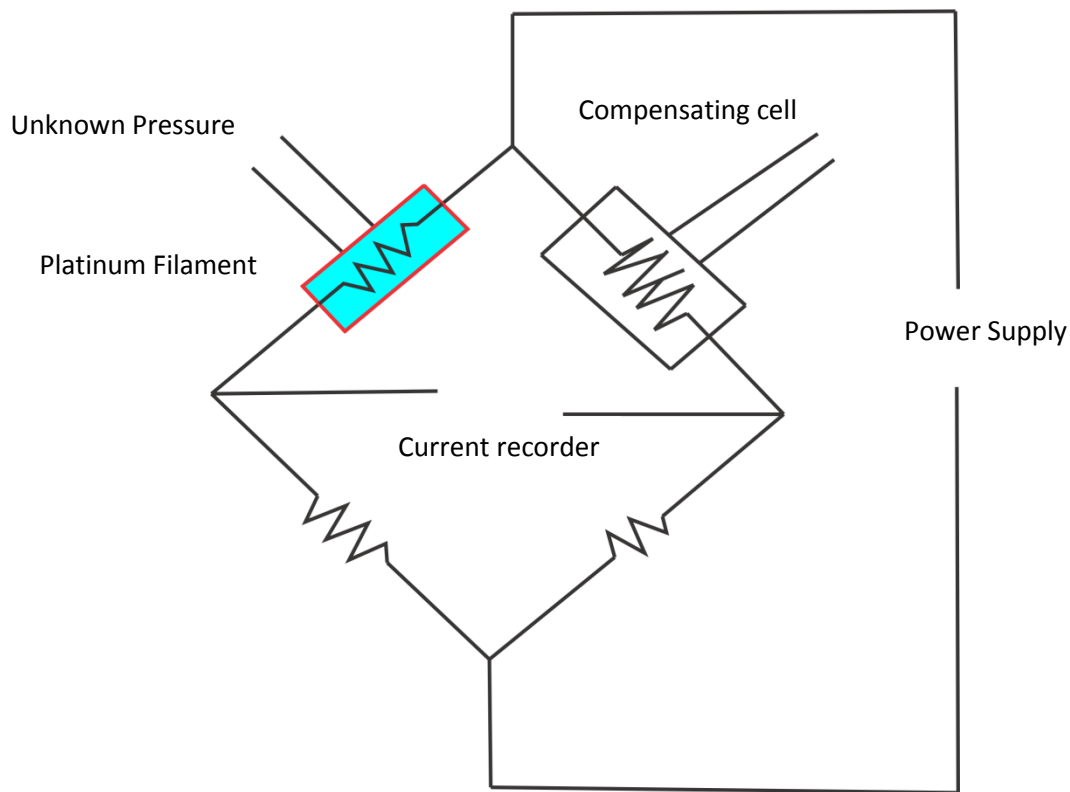
Figure 2.9 Pirani Gauge

2.9 Noise Reduction

Noise reduction is necessary for taking STM measurements. The tip of the STM goes very close to the sample. Without noise reduction a stable measurement is not possible with STM. Noise reduction is achieved in three ways. LT STM stage is hanged using three soft springs whose resonance frequency is 2 Hz. Vibrations of suspension system are intercepted using nearly non periodic eddy current damping mechanism. There are permanent magnets fixed at the bottom of the LHe cryostat. A ring of metal damping U profile surrounds LT STM stage which comes down between permanent magnets.

2.10 Tip Preparation

For the STM measurements we can use either Pt-Ir tip or W tip. W tip were used in the experiments which was made by electrochemical etching. A diagram of the etching circuit is given in figure 2.10. Ideally a tip with single atom end gets formed after the etching process. Optical microscope image of W tip is given in figure 2.11. For etching 2M NaOH solution was prepared by adding 8g of NaOH in 20 ml of water. The voltage applied was 4 V.
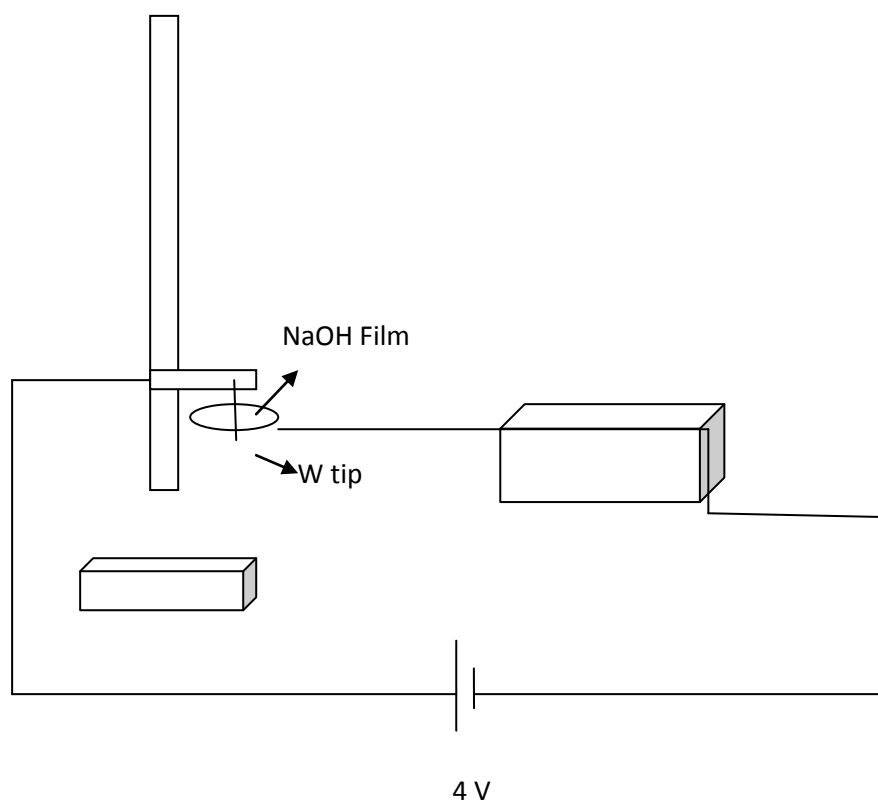

NaOH Film

W tip

4 V

Figure 2.10 Electro Chemical Etching Circuit

2.11 Sputtering and Annealing

Sputtering is the process by which particles will be ejected from a solid surface by bombarding it with charged particles. Argon gas was used for sputtering the sample. A high bias will be applied to the argon gun which ionises argon gas and accelerates them towards the sample. Annealing refers to heating the sample. Tungsten filament attached to the manipulator arm was used for this purpose. It can either evaporate molecules from the substrate or reconstruct the crystal surfaces.

2.12 Molecular Evaporator

A molecular evaporator was designed for the physical vapour deposition of boron powder in the UHV chamber. An image of the molecular evaporator is given below (Figure 2.11). Alumina crucible is attached to feed through via a clamping pin. Thermo couple is attached to the crucible which measures the temperature of the crucible during deposition. Once the connections were made boron powder was added to the crucible.
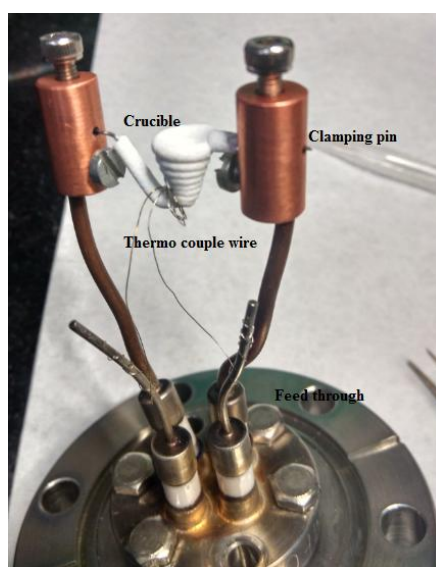

Figure 2.11 A home built molecular evaporator

2.13 Atomic Force Microscope (AFM)

Atomic force microscope (AFM) is a probing microscope which can be used for imaging nano structures. Figure 2.13 shows the schematic of an AFM. It consists of a Silicon or silicon nitride cantilever. When the cantilever scans along the surface it will have deflections according to Hooke's law. Mechanical contact force, electrostatic forces, magnetic forces, van der Waal's force, etc. can be measured using AFM. It has different modes of operations, namely contact mode, tapping mode and non contact mode.

Contact mode: In this mode cantilever will be dragged above the surface of a soft material. Cantilevers with low spring constant are used for this purpose.

Tapping mode: Tapping mode is achieved by oscillating cantilever at or near its resonance frequency. This is the most used mode for scanning samples.

Non-contact mode: As the name suggests the cantilever does not touch the sample surface in this mode. It oscillates at or above its resonance frequency. Sample or cantilever damage will be lesser in this mode.
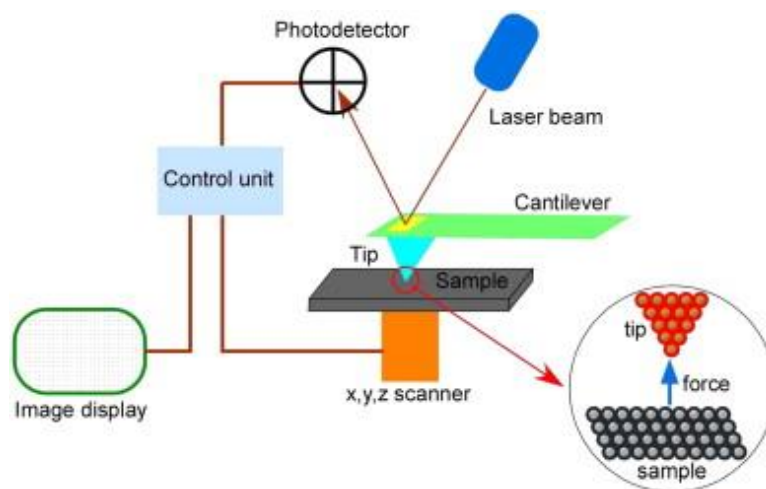

Figure 2.12 A schematic showing the setup of AFM[25]

2.14 Energy Dispersive X-Ray Spectroscopy (EDAX)

EDAX is used to analyse the elemental composition of a given sample. EDAX method was used to verify the presence of boron over Au substrate after deposition. X-Ray beams or charged particles such as electrons or protons get bombarded with the sample, which excite electrons from the sample atoms. These electronic transitions produce X- Rays. Energy dispersive X- Ray spectrometer is used to measure the energy and number of X- Rays emitted. This gives an idea about the elemental composition of the sample.

In my experiment I have used field emission scanning electron microscope (FESEM) for doing EDAX. FESEM uses an electron beam which is produced using field emission gun. Electron beam is focussed using electromagnetic lenses associated with the instrument. Focussed beam falls on the sample and ejects secondary electrons. These secondary electrons are collected and converted to signals. The signal conversion is based on the velocities and angles of secondary electrons. Image of the sample is produced from the signals.

2.15 Sample Preparation

Cleaning Au (111): Gold coated mica (Sigma Aldrich, 2000 A$^{°}$ coating) was used as the substrate throughout the experiments which has a Au(111) surface. Initially gold coated mica was spot welded to the tantalum plate. Au (111) substrate was cleaned using repeated sputter annealing cycles. After cleaning Au (111) surface was checked using STM.

Depositing Boron: Boron powder (99.999% pure) was added to the home built molecular evaporator which was described earlier. This acts as the source of boron during deposition. Before depositing boron, degassing of the boron source was carried out. During the deposition constant power source was used to provide the power supply to the crucible. Deposition was done when the crucible reached a particular temperature. Exposure time of the substrate to the boron flux was also controlled during deposition. Trials were also carried out by changing the substrate temperature. After deposition the sample was transferred to the STM for further analysis.

RESULTS AND DISCUSSIONS

3.1 Cleaning Bare Au(111)

The work started by preparing a Au(111) sample for deposition of boron. At the beginning of the work AFM imaging of gold coated mica was done at room temperature. It was done after a flash annealing of the gold coated mica using a Bunsen burner. This was done as a quick check of the surface of gold coated mica. Following is the AFM image for gold sample. Tapping mode was used for AFM imaging.
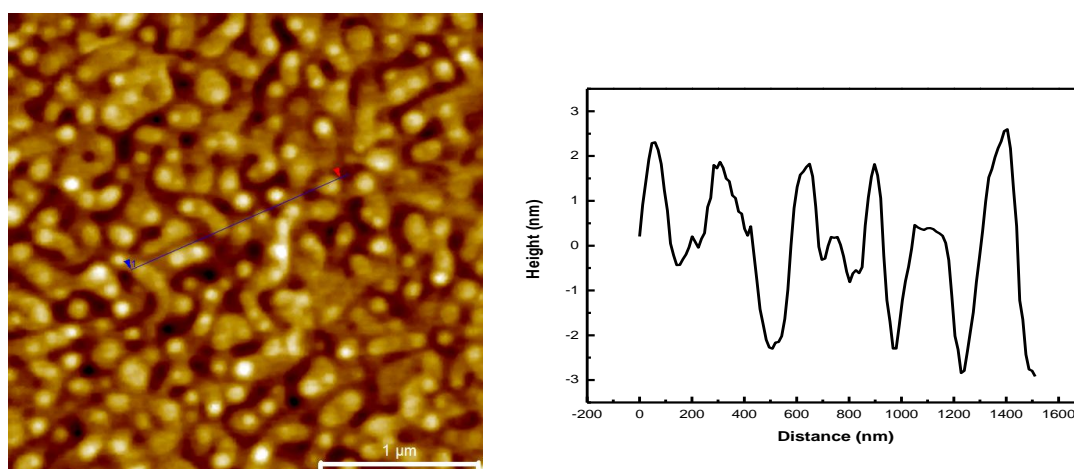

Figure 3.1 AFM image of Au(111) and the line profile of the same.

Line graph shows the height variations along the blue line in the topography image. The image and the line profile suggest that there are no impurities and there are enough flat areas to work with.

In UHV Sputtering and annealing cycles were done to clean the Au sample. Annealing was done at 500^0C and sputtering was done using 1keV beam energy and 1µA emission current. Repeated cycles of sputtering and annealing cleaned the Au surface. After cleaning the Au surface was scanned using scanning tunnelling microscope at 77K. Following images were obtained from clean gold. These images show atomic steps, herringbone reconstructions and atomic resolution of Au(111) surface. All the STM images were taken using constant current mode.

Gold has a face centred cubic lattice. Reconstruction of the (111) plane of Au is termed as herringbone reconstruction. The model for herringbone reconstruction has one stacking fault

per unit cell. The (111) surface of gold has hexagonal close packed ((ABA) stacking) as well as face centred regions ((ABC) stacking). They are connected by two partial schockly dislocations and these dislocations add 0.5 atoms each. Thus it gives rise to one extra atom per reconstructed unit cell and results in an average 4.2 % contraction of the surface layer along [110] direction. Model for reconstruction of Au(111) surface is given in the following figure. [26]
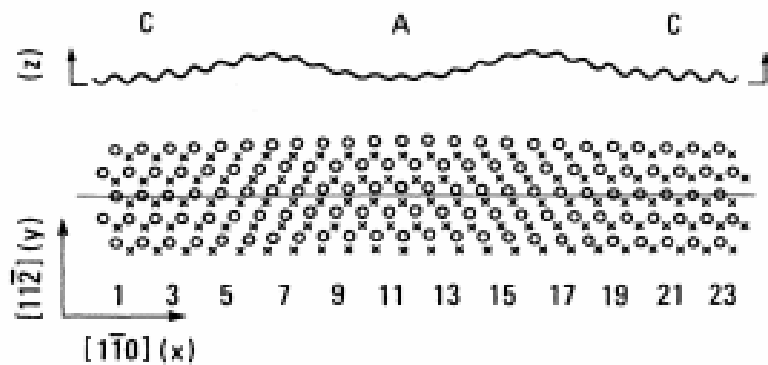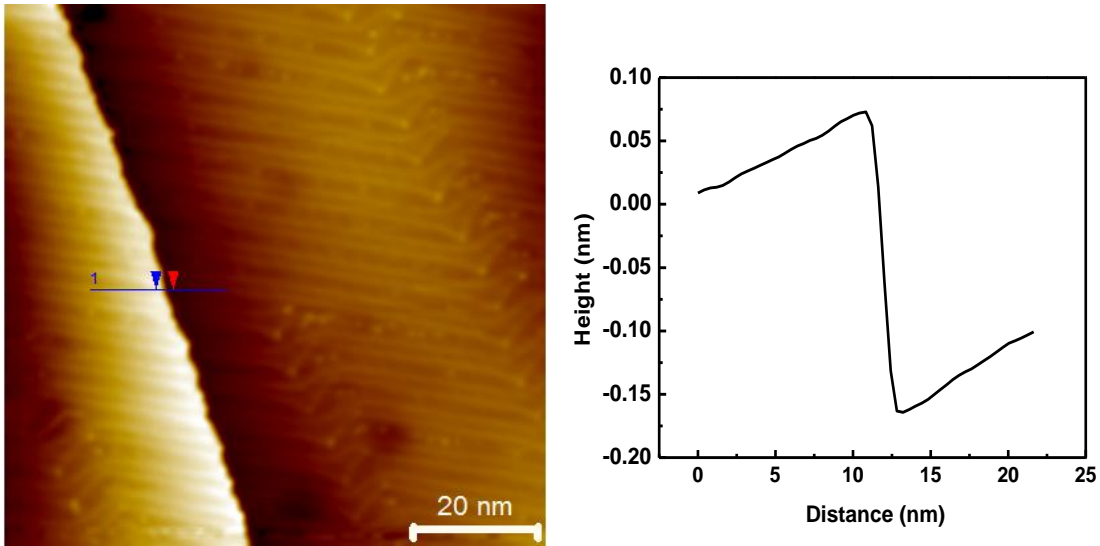

Figure 3.2 Diagram explaining herringbone reconstructions [26]

Open circles represent atoms on the top layer which is reconstructed and crosses the atoms on the second layer. Region A has hcp arrangement and C has fcc arrangement. This models the herringbone reconstruction of gold.
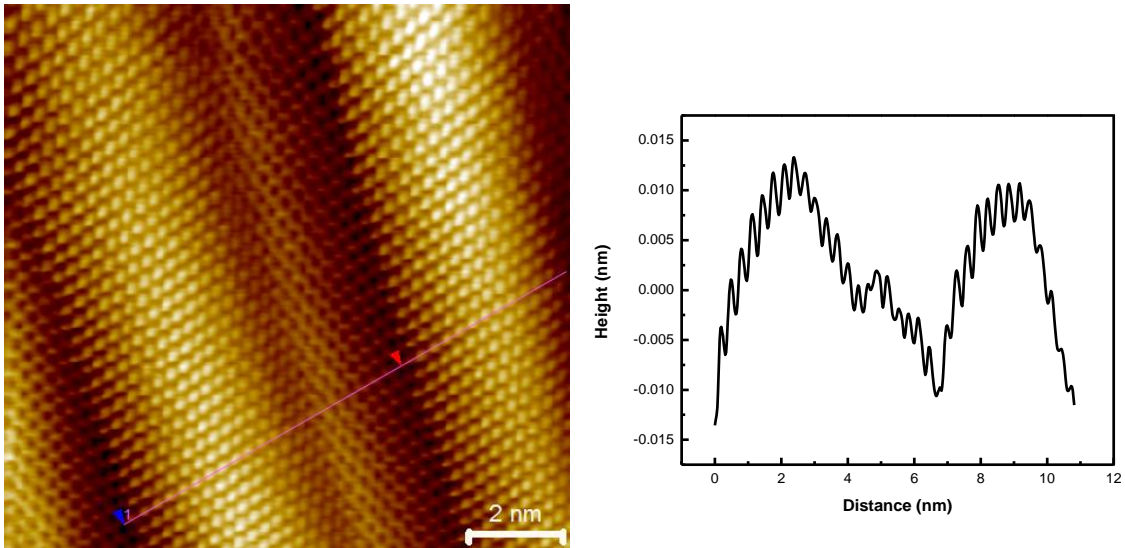
V = 1V, I = 80pA

Figure 3.3 STM image of Au(111) surface with mono atomic steps. Plot showing line profile along mono atomic step of Au(111). Step size measured from this graph is 2.36 A˚.
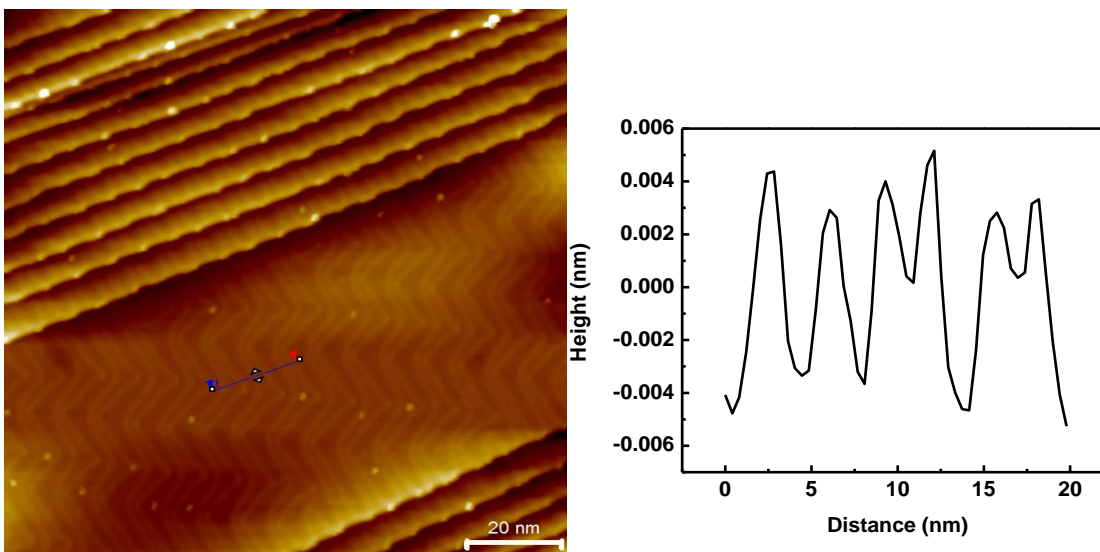
V = 1.2 V, I = 100 pA

Figure 3.4 STM image of Au(111) with herringbone reconstructions and monno atomic steps. The distance between two hcp regions of herringbone is aroung 6 nm.

V = 0.5 V, I = 500 pA

Figure 3.5 Atomic resolution image of Au(111) surface and the line profile of the same.

Four trials of boron deposition were carried out. Different parameters like temperature and pressure of deposition, substrate temperature and exposure time were changed from one trial to another. Detailed description of each trial is as follows.

3.2 The First Trial

In the first trial almost every parameters were unknown. The boron source was heated to 740^0C and Au(111), held at room temperature was exposed to the source for 30 seconds when the pressure was $8*10^{-7}$ mbar. The STM image after the deposition is shown in figure 3.6
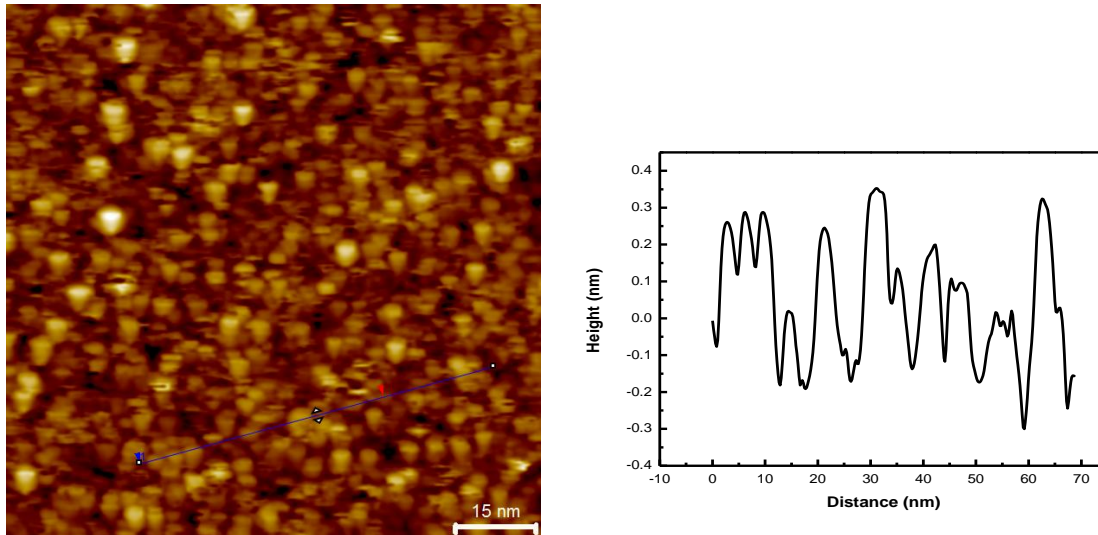
V = -2V, I = 80pA

Figure 3.6 STM image of boron clusters after the first deposition. Line profile shows the topographic variations of the same.

The line profile showed large surface variations which suggested that there was a high deposition of boron over gold. No bare substrate was seen in any of the scans.

This trial gave an idea about the temperature of deposition and exposure time. Next time deposition was done at lower temperature and with lesser exposure time.

Presence of boron over Au(111) was confirmed using energy dispersive X-Ray analysis (EDAX) technique. The sample was taken out of UHV after the STM imaging and then the EDAX was done. 25.59 percentage of boron atoms was the estimation by EDAX technique, which confirmed that boron is getting deposited on Au(111) during physical vapour deposition. EDAX data is given below.
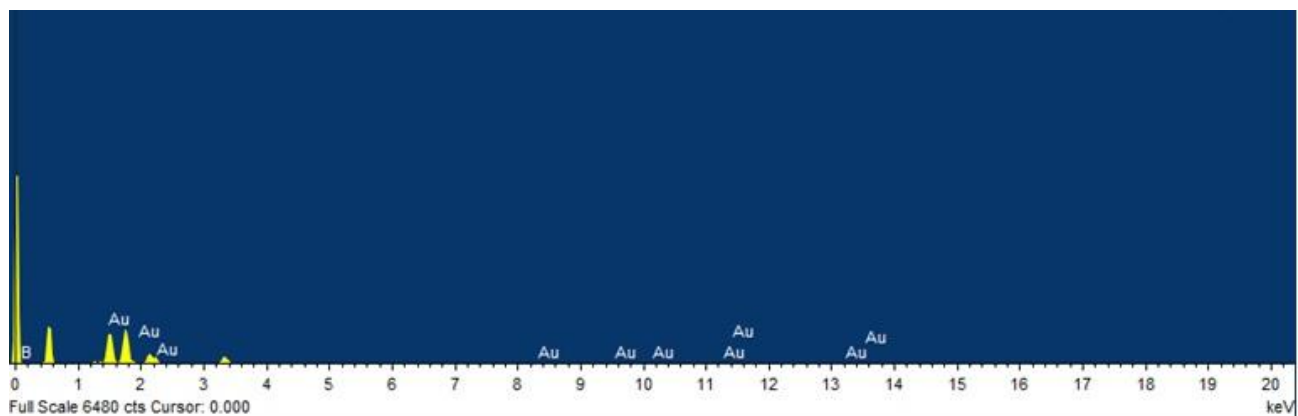
Figure 3.7 EDAX data

Element	Weight %	Atomic %
B	1.85	25.59
Au	98.15	74.41

Table 3.1 EDAX data showing percentage of elements present on the surface of the sample
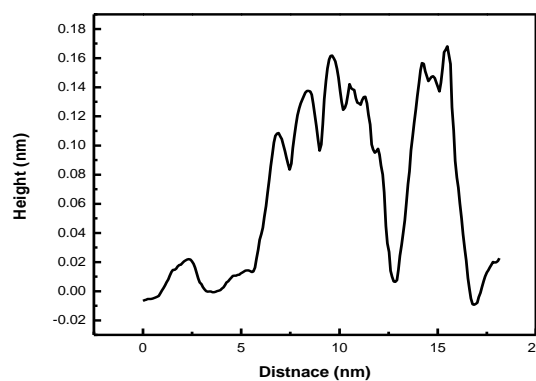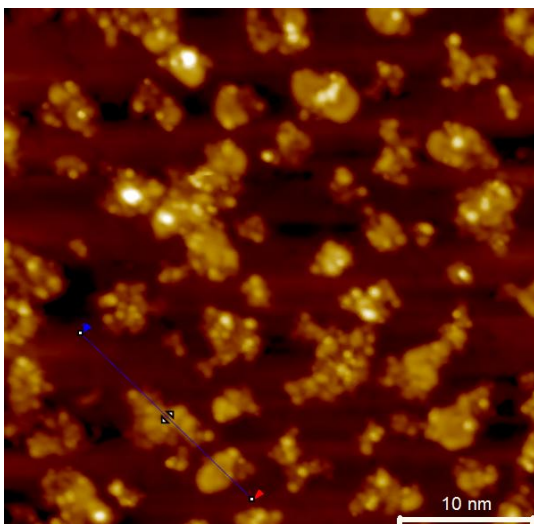
3.3 Second Trial

In second trial the temperature of deposition was $675^{0}C$ and the pressure was $6.6*10^{-8}$ mbar. Exposure time was reduced to 10 seconds. STM images show some signs of substrate below the deposits. This was a controlled deposition compared to the first one.
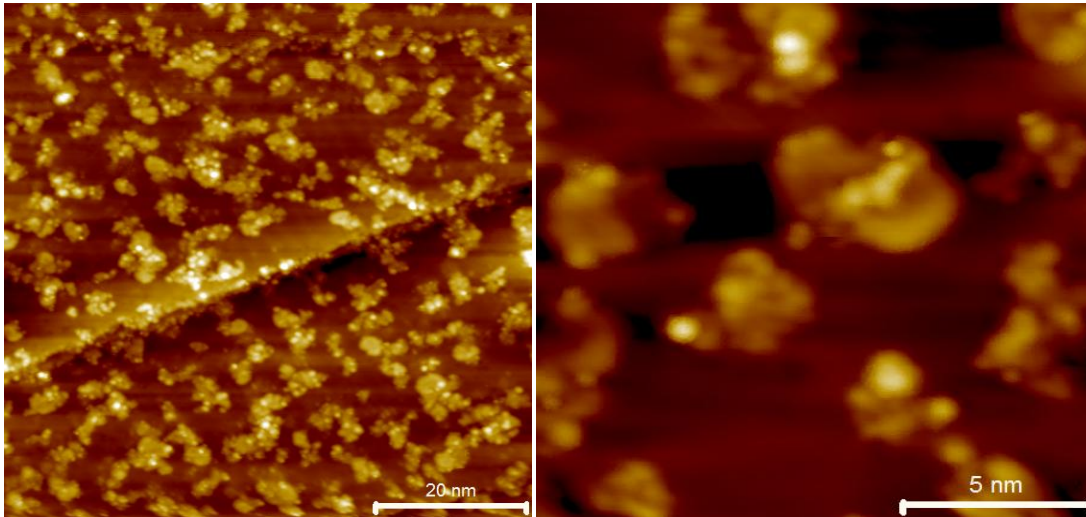
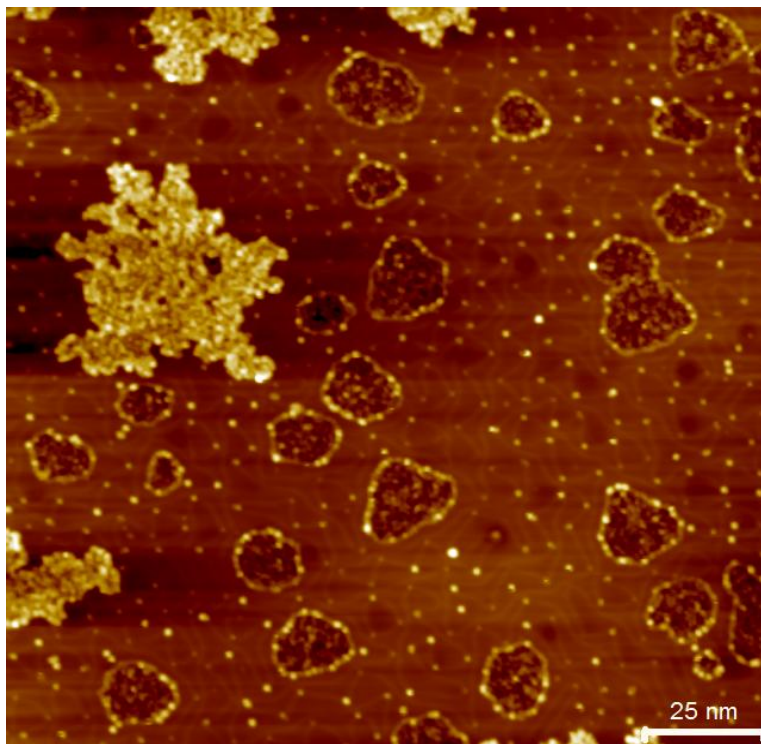**V = 1.5V, I = 80pA**

V= 0.8 V, I = 1 nA

V = 0.8V, I = 600pA

Figure 3.8 STM images showing boron clusters over Au(111) after second deposition. The line profile shows that there was a more planar deposition in the second trial.

3.4 Third Trial

This time Boron was deposited at 650^0C for 7 seconds and the pressure was $3.2*10^{-7}$ mbar. Substrate was kept at 300^0C during deposition.
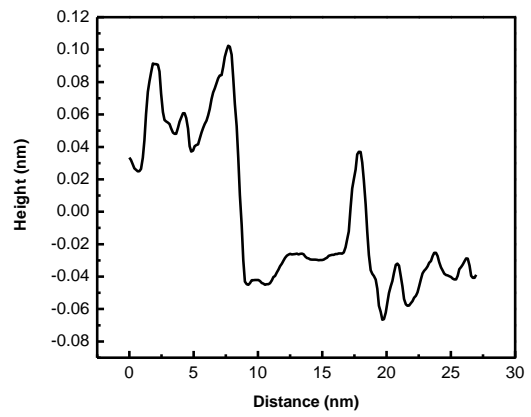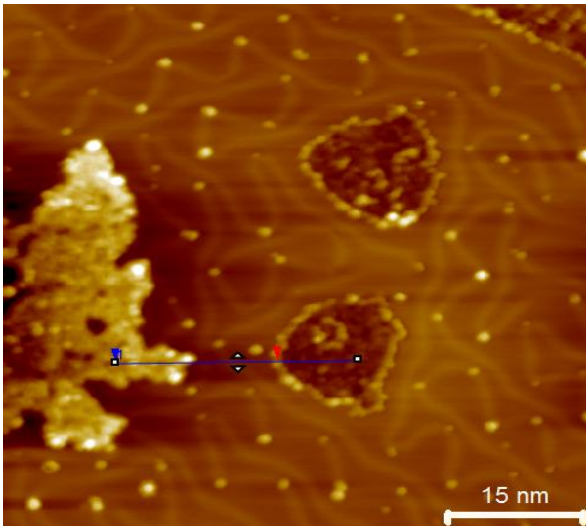

V = 2V, I = 50pA

Figure 3.9 STM image of boron islands and dark patches over Au(111)
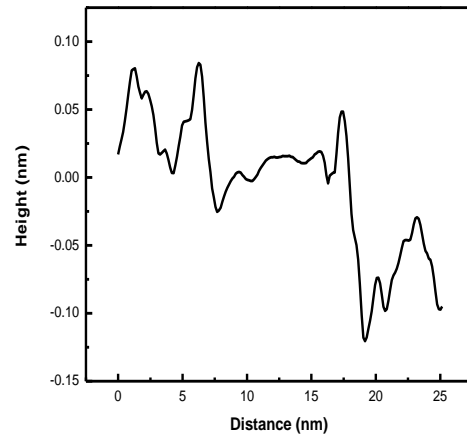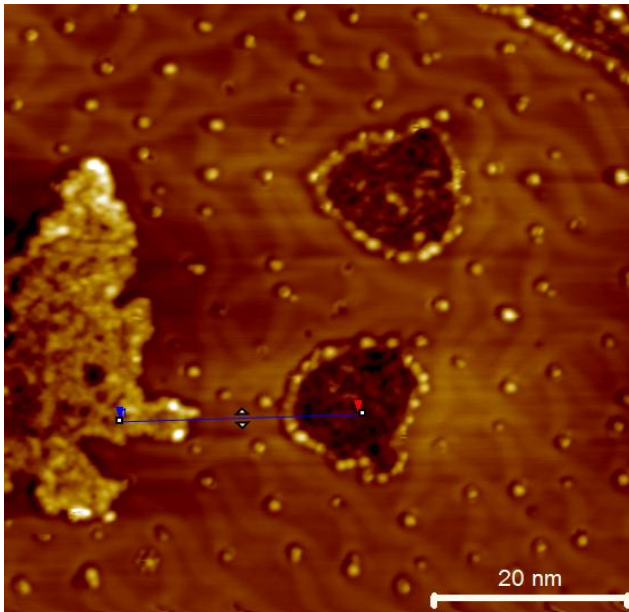
Island like deposits and dark patches were observed on the Au(111) substrate. Au(111) surface could be seen with herringbone reconstructions. Dark patch like structure had a lesser height compared to the substrate. Boron sheets over Ag(111) showed a similar morphology near Fermi level and at positive bias, where as it had given positive height at high negative bias..[19] This can be related to the integrated density of states corresponding to each voltage for both Ag substrate and the boron islands. Similarly, voltage dependent imaging was done to see how the topography of boron islands, dark patches and Au substrate changes with bias. The following images were taken at the same area for -2.5V, - 2V, 2V and 2.5V. These images did not show any considerable change in morphology of patches or islands with change in bias. All voltages gave dark patches with height lesser than the substrate.
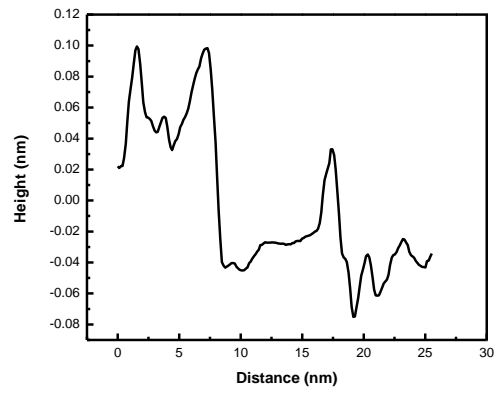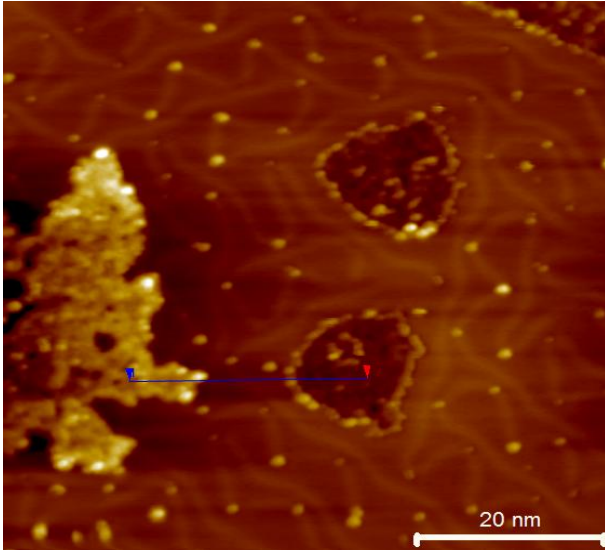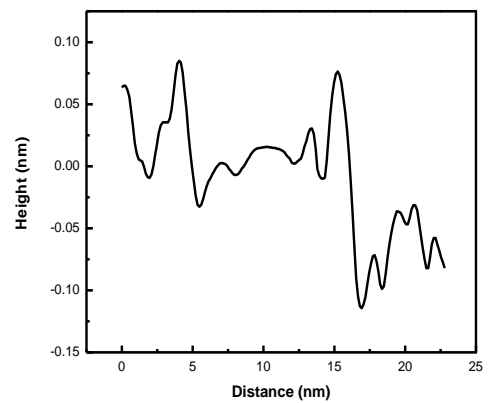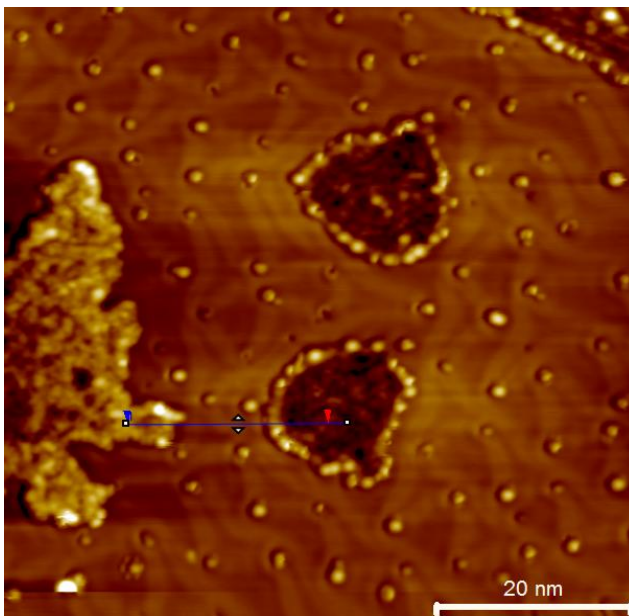
V = -2.5 V, I = 50 pA

V = -2V, I = 50pA

V = 2V, I = 50pA

V = 2.5V, I = 50pA

Figure 3.10 STM images for boron islands and dark patches over Au(111) for different applied biases. Line graph is also given with each image.

Herringbone reconstruction of Au(111) was clearly visible. Island like deposits and dark patches were not atomically flat and thus it was unable to get an atomic resolution image on them. Herring bone reconstruction looked different from the herringbone reconstructions on clean Au(111) surface. The distance between two hcp regions also got changed in some areas. In areas with dark patches herringbone was completely removed. There are similar observations known as lifting of herringbone reconstructions in gold when organic molecules like Trimethylphosphine are adsorbed on to the gold surface.[27]

After the analysis using STM the sample was annealed at 450^0C for 30 minutes. Annealing removed all the dark patches and boron clusters were spread across Au(111) surface.

3.5 Fourth Trial

Fourth deposition was carried out by increasing the substrate temperature to 400^0C. Temperature and pressure during deposition were 650^0C and 8.8*10-8 mbar. Exposure time was 10 seconds.
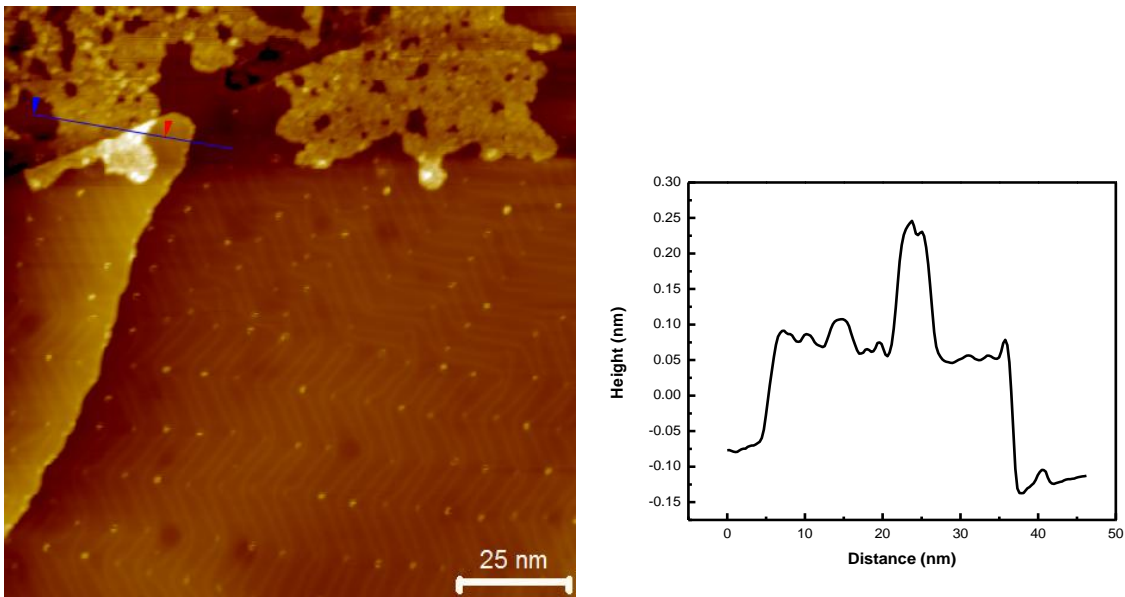
V = 1.4V, I= 80pA

Figure 3.11 STM image with boron island over Au(111) after fourth deposition. There was no sign of any patch like structures over Au(111)

This trial gave rise to island like deposits and they were not atomically flat. Gold substrate and herringbone reconstructions were visible. Unlike third deposition dark patches did not get formed in this trial. Further annealing at 450 degree Celsius for 10 minutes produced random clusters on the substrate.

Table 3.1 summarizes the average of topographic variations of sample surface in each trial. The values are found by averaging 10 random height measurements from each trial.

Trial Number	Range of topographic variations(nm)
1	0.67 nm
2	0.21 nm
3	0.12 nm
4	0.10 nm

Table 3.2 Topographic variations of the sample

As evident from the table the fourth, third and second depositions were more planar compared to the first deposition.

CONCLUSIONS AND OUTLOOK

Efforts were made to prepare borophene on Au(111) substrate. Au(111) was cleaned using repeated sputter annealing cycles. Cleaned Au(111) was characterised atomically using STM . Boron deposition trials were carried out. Parameters like substrate temperature, temperature of evaporation and exposure time were tuned during deposition of boron. More planar structures got formed when substrate was kept at 300˚C and 400˚C, but was lacking a well ordered atomic scale structure.

In future boron deposition trials have to be carried out by reducing the boron flux and with lesser exposure time. This can possibly bring about mono layer deposition of boron over Au(111). Substrate temperature will also play a critical role in the formation of borophene. More trials are needed to be done for optimizing the substrate temperature for the growth of borophene over Au(111). Once borophene gets formed its local electronic properties and atomic scale structure can be studied in detail using STM.

BIBILIOGRAPHY

(1) David Mohtasham.Review article – Renewable energies. Energy Procedia 74, 1289-1297(2015)

(2) A. K. Geim, K. S. Noveselov. The rise of graphene. Nature materials 6, 183-191 (2007)

(3) Atkin's Inorganic Chemistry, 5th Edition

(4) Woods, W.G. An introduction to boron: history, sources, uses, and chemistry. Environ. Health Perspect 102, 5-11 (1994)

(5) Albert, B. & Hillebrecht, H. Boron: elementary challenge for experimenters and theoreticians. Angew. Chem. Int. Ed. 48, 8640-8668 (2009)

(6) T. Ogitsu, E. Schwegler, G. Galli, β-Rhombohedral boron: At the crossroads of the chemistry of boron and the physics of frustration. Chem. Rev. **113**, 3425–3449 (2013).

(7) A. R. Oganov, J. H. Chen, C. Gatti, Y. Z. Ma, Y. M. Ma, C. W. Glass, Z. X. Liu, T. Yu, O. O. Kurakevych, and V. L. Solozhenko, Nature (London) 457, 863 (2009).

(8) H.-J. Zhai, Y. F. Zhao, W. L. Li, Q. Chen, H. Bai, H. S. Hu, Z. A. Piazza, W. J. Tian, H. G. Lu, Y. B. Wu, Y. W.Mu, G. F. Wei, Z. P. Liu, J. Li, S. D. Li, L. S. Wang, Observation of an all-boron fullerene. Nat. Chem. **6**,727–731 (2014).

(9) Z. A. Piazza, H. S. Hu, W. L. Li, Y. F. Zhao, J. Li, L. S. Wang, Planar hexagonal B(36) as a potential basis for extended single-atom layer boron sheets. Nat. Commun. **5**, 3113 (2014).

(10) I. Boustani, Phy. Rev.B, 16426-16438, Systematic ab initio investigation of bare boron clusters: Determination of the geometry and electronic structures of Bn (n=2 -14) (1997)

(11) H. Tang, S. Ismail-Beigi, Novel precursors for boron nanotubes: The competition of two-center and three-center bonding in boron sheets. The competition of two-center and three-center bonding in boron sheets Phys. Rev. Lett. **99**, 115501 (2007).

(12) X.-F. Zhou, X. Dong, A. R. Oganov, Q. Zhu, Y. Tian, H.-T. Wang, Semimetallic two-dimensional boron allotrope with massless Dirac fermions. Phys. Rev. Lett. **112**, 085502 (2014).

(13) K. C. Lau, R. Pandey, Stability and electronic properties of atomistically-engineered 2D boron sheets.J. Phys. Chem. C **111**, 2906–2912 (2007)

(14) E. S. Penev, S. Bhowmick, A. Sadrzadeh, B. I. Yakobson, Polymorphism of two-dimensional boron.Nano Lett. **12**, 2441–2445 (2012).

(15) Y. Liu, E. S. Penev, B. I. Yakobson, Probing the synthesis of two-dimensional boron by first-principles computations. Angew. Chem. Int. Ed. **52**, 3156–3159 (2013).

(16) H. Liu, J. Gao, J. Zhao, From boron cluster to two-dimensional boron sheet on Cu(111) surface: Growth mechanism and hole formation. Sci. Rep. **3**, 3238 (2013).

(17) Liu, F. et.al. Metal-like single crystalline boron nanotubes: synthesis and in situ study on electric transport and field emission properties. J. Mater. Chem. 20, 2197-2205 (2010)

(18) Andrew J. Mannix , Xiang- Feng Zhou, Brick Kiraly, et.al. Synthesisi of borophene: anisotropic two-dimensional boron polymorph, Science, DOI:10.1126/science.aad1080 (2015)

(19) Baojie Feng, Jin Zhang, et.al. Experimental realization od two dimensional boron sheets. Nature Chemistry 8, 563-568 (2016)

(20) Zhuhua Zhang, Andrew J Mannix, et.al. Substrate induced nanoscale undulations of borophene over silver. Nano Letters, DOI:10.1021/acs.nanolett.6b03349 (2016)

(21) Baojie Feng, Osamu Sugino, et.al. Dirac fermions in borophene. Physical Review Letters, PRL118,096401 (2017)

(22) Xiaojun Wu, et.al. Two-Dimensional Boron Monolayer Sheets, ACS NANO (2012)

(23) Introduction to scanning tunnelling microscope, Second edition, C. Julian Chen

(24) Modern Vacuum Practice, Third Edition, Negel Harris

(25) Aparna Deshpande, Brian J. LeRoy. Scanning probe microscopy of graphene. Physica E : Low-dimensional Systems and Nanostructures, volume 44, issue 4, 743-759 (2012)

(26) Ch. Woll, S. Chiang, et.al. Determination of atom positions at stacking- fault dislocations on Au(111) by scanning tunnelling microscopy. Physical Review B, Volume 39, Number 11(1989)

(27) April D. Jewell, Heather L. Tearney and E. Charles H. Sykes. Gently lifting gold's herringbone reconstruction: Trimethylphosphine on Au(111). Physical Review B 82, 205401 (2010)